

Mary Ann Jenkins¹ * Adam Kochanski² Steven K. Krueger²

¹York University, Toronto, Canada

²University of Utah, Salt Lake City, Utah

1. INTRODUCTION

Firelines tend to take on a “parabolic” shape when burning in an environmental wind field that is steady, constant with height, and directed perpendicular to the fireline (Cheney et al., 1993). Clark et al. (1996a) and Clark et al. (1996b) were two of the earliest efforts to employ a numerical prognostic cloud-resolving model coupled with an operational fire behavior model to study in a systematic way the sensitivity of fireline stability, geometry, and spread rate to an ambient wind field of this type.

Figure 1 is a schematic of the idealized structure of the near-surface convergence pattern in the vicinity of a fire as described by Clark et al. (1996a). Clark et al. (1996a) explained the parabolic shape by considering the projection of the convergence in the near-surface flow produced by the convection column of the fire. When no ambient wind is present, a vertically-oriented convection column draws low-level air equally from all sides. When an ambient wind is present, the horizontal structure of the east-west component of the near-surface flow displaced horizontally from the convection column has a bell- or parabolic- like shape with a maximum amplitude centered in the north-south direction of the cell.

According to Clark et al. (1996a), the effect of downstream tilting of the convection column by a background wind is to shift the center of the low-level convergence pattern downstream, ahead of the fire front; the faster the ambient wind, the stronger the tilt, and the farther downstream the center of the convergence zone is positioned. Clark et al. (1996a)’s explanation for the parabolic fireline shape could be called the “kinematic” explanation. However, because the magnitude of the constant background wind — and that of the near-surface wind — differed between experiments, it was not possible for Clark et al. (1996a) and Clark et al. (1996b) to decide if or how much the downstream projection of the convergence zone depended on the strength of the upstream mean near-surface wind as opposed to near-surface wind features at the fire front that were the result of interactions of the convection column with the above-surface wind conditions.

The questions therefore that we wish to examine here are as follows. Can the propagation and perimeter of a wildfire be forecast accurately based on solely the strength and direction of the mean upstream near-surface wind? A kinematic explanation is concerned only with motion without reference to the forces responsible for the motion. Is there a distinctive flow feature that involves a dynamical force? The answers to these questions are important to operational fire spread forecasting. We demonstrate that the vertical wind structure, not just an upstream temporally-constant spatially-averaged near-surface wind (i.e., at “mid-flame” height for example in the Rothermel model, as often applied in operations), is needed to forecast fire behavior and propagation. And we attempt to show that both steady-state and non-steady-state propagation of the fire perimeter are accompanied by certain flow features. The flow features important to fireline propagation that we discuss are described in the following section, where the development of persistent, long-lasting vertical vortices is proposed as the fluid-dynamical feature associated with forcing and acceleration of the flow.

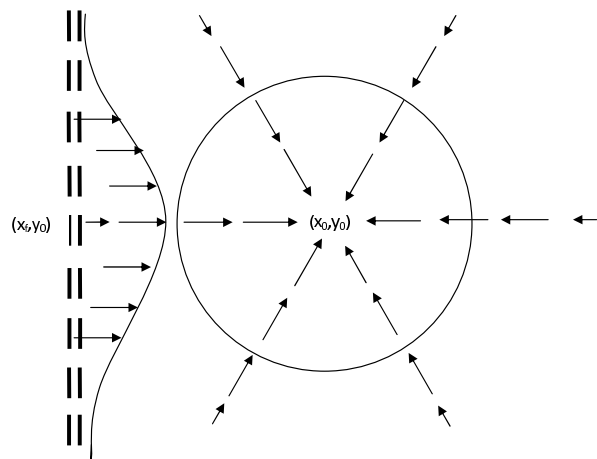


Figure 1: Idealized structure according to Clark et al. (1996a) of the near-surface convergence pattern in the vicinity of fire. The background wind is blowing from left to right. See text for explanation.

* Corresponding author address: Department of Earth and Space Science and Engineering, York University, Toronto, ON, Canada, M3J 1P3. E-mail: maj@yorku.ca

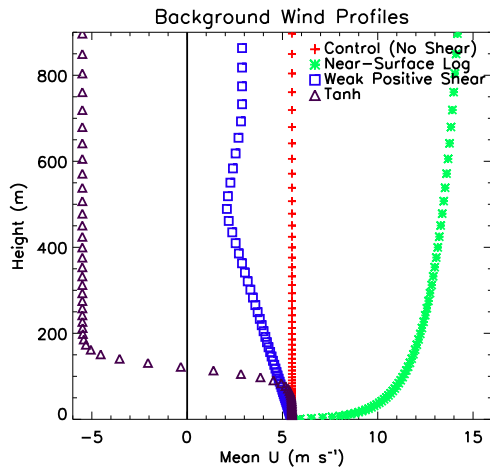


Figure 2: Vertical profiles of the $\bar{u}(z)$, background wind, used in coupled WRF-SFIRE experiments CONTROL (red plus signs), LOG (green asterisks), SHEAR (blue squares), and TANH (dark purple triangles). See text for further explanation.

2. NUMERICAL EXPERIMENTAL SET-UP

The Large-Eddy Simulation (LES) version of the WRF (Weather Research and Forecasting) model (Wang et al., 2009) coupled with SFIRE, the wildland surface fire module (Mandel et al., 2008, 2011), was used to simulate four moving surface grass fires, burning in uniform fuel on level terrain, initialized as straight firelines perpendicular to the direction of background the wind. Each simulation lasted 15 minutes. Initial fireline length and width were 400 and 20 m, respectively, and fuel load was 0.626 kg m^{-2} . The background temperature was a uniform potential temperature of 300K.

In the WRF-SFIRE model domain a Cartesian (x,y,z) grid mesh of $(320,160,81)$ nodes was used where the horizontal grids intervals were $(\Delta x, \Delta y) = 20 \text{ m}$, making the (x,y,z) domain dimensions $(6400 \text{ m}, 3200 \text{ m}, 3900 \text{ m})$. For the WRF-SFIRE's surface fire grid (Mandel et al., 2008, 2011), the fire-to-atmosphere refinement ratio was 10, which translates into fire domain grid intervals of $(\Delta x, \Delta y)_f = 2 \text{ m}$. A hyperbolically-stretched vertical grid was used, with a minimum vertical Δz grid size of 1.5 m in the first grid level. The model time step was 0.02 s. Open boundary conditions (Klemp and Lilly, 1978) were applied on the lateral and top boundaries.

There are four simulations, CONTROL, LOG, SHEAR, and TANH, and Figure 2 shows the westerly background wind as a function of height that was ap-

plied at the inflow boundary for each experiment. The environmental surface wind speed in each case was 5.5 m s^{-1} . With the exception of the TANH simulation, each initial fireline was located 2000 m in the positive x (east-west) direction. In the TANH fire, the initial fireline was located 4000 m in the positive x direction. All firelines were centered in the y (north-south) direction.

CONTROL illustrates the evolution of a grassfire burning in an environment of constant westerly flow with no above-surface vertical wind shear (red plus signs in Figure 2) and serves as the prototype for comparison with the other simulations. To insure that the impact of surface drag on the in-flow wind profiles is not factor in the flow features observed in the simulations, surface roughness was set to zero. In this way, the CONTROL fire represents a “tool” that considers ONLY an upstream ambient 5.5 m/s , constant with height and time, wind. With no surface drag and open boundary condition, the inlet upstream wind profiles (Figure 2) remain steady throughout the time span of the simulations.

In LOG the vertical distribution of the westerly background inflow (green asterisks in Figure 2) is prescribed by the log-linear wind profile based on a near-surface wind of 5.5 m s^{-1} and a roughness height of 0.036 m (for grass). A slightly negative linear-sheared background wind profile (where the wind blows faster at the surface than aloft) is used in SHEAR (blue squares in Figure 2). In TANH the low-level shear in the background wind profile is strongly negative (dark purple triangles in Figure 2); it varies from 5 m s^{-1} near the ground, changes sign at $z = 250 \text{ m}$, and is asymptotic to -5 m s^{-1} aloft. Each fire's plume experiences different upper-level wind strengths; the magnitude of the upper-level zonal flow is strongest in the LOG fire ($\sim 15 \text{ m s}^{-1}$), weakest in the SHEAR fire ($\sim 3 \text{ m s}^{-1}$), and moderate ($\sim 5.5 \text{ m s}^{-1}$) in the CONTROL and TANH fires.

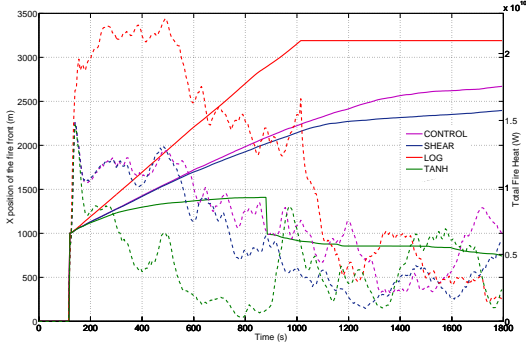


Figure 3: Time series of the fire front positions in the x direction (solid lines), and the instantaneous total heat-release rates in the fire domain (dashed lines), for CONTROL (purple), SHEAR (navy), LOG (red) and TANH (green) fires.

3. FLOW FEATURES

A few basic features associated with the evolution of the surface flow are used to illustrate the impacts that the different upstream above-surface background wind fields (Figure 2) have on the spread of a fireline. In the following, subscripts (x,y) denote differentiation with respect to (x,y) and superscript z denotes a vertical vector component.

Near-surface flow due to fire/atmosphere interactions is described by the magnitude of the perturbed horizontal wind vector, which expressed mathematically is

$$|\vec{V}'_H| = \sqrt{(u - \bar{u})^2 + v^2}, \quad (1)$$

where $\vec{V}_H = (u\hat{i}, v\hat{j})$, is the horizontal (denoted by subscript H) wind vector, (u,v) are (x,y) components of the flow, and (\hat{i}, \hat{j}) are (x,y) unit vectors in the Cartesian coordinate system. The overbar $(\bar{\quad})$ denotes the base state or mean state, and $\bar{u}(z)$ represents the background wind profile that is a function of height z only. The prime ($'$) denotes the perturbation or deviation/fluctuation from the base state. Here $u = \bar{u}(z) + u'$ and $v = v'$. It is $\bar{u}(z)$ for each numerical experiment that is displayed in Figure 2.

Separation and coming together of flow parcels in the x - y plane are described by horizontal divergence, δ , which expressed mathematically is

$$\delta = \nabla_H \cdot \vec{V} = u'_x + v'_y, \quad (2)$$

where $\delta > 0$ signifies divergence and $\delta < 0$ signifies convergence of flow parcels.

The spin or rotation of flow parcels in the x - y plane is described by ζ^z , the component of the vorticity (i.e., fluid rotation at a point) vector in the vertical (z) direction, which expressed mathematically is

$$\zeta^z = v'_x - u'_y. \quad (3)$$

One reason vorticity is often a distinctive feature in atmospheric flows is its attribute of persistence. When a region of fluid acquires vorticity, this flow pattern tends to last a relatively long time compared to other flow patterns on the same scale. Vortices arise within a flow containing vorticity and tend to be associated with discrete, nearly circular extrema of vorticity. In a wildfire it is not unusual for the magnitude of vertical vorticity in a vortex to reach that for supercell-storm tornadoes, which is approximately 0.3 to 1.2 s^{-1} (Bluestein et al., 1993).

Vorticity development is a natural phenomenon in convection, and many studies have used the relationship,

$$p'_d \propto -|\vec{\Omega}|^2, \quad (4)$$

where p'_d is the dynamic pressure perturbation and $\vec{\Omega}$ is the three-dimensional vorticity vector, defined as $\vec{\Omega} = \nabla \times \vec{V}$, the curl or vector cross-product of \vec{V} , where $\vec{V} = (u\hat{i}, v\hat{j}, w\hat{k})$ is the three-dimensional velocity vector. Vertical vorticity ζ^z in Equation (3) is equal to $\hat{k} \cdot \vec{\Omega}$, where \hat{k} is the unit vector in the vertical z direction. The p'_d is so named because it develops from vorticity as part of the flow dynamics; it is not a hydrostatic pressure perturbation.

Equation (4) indicates that, qualitatively, pure rotation, of any sense and in any direction, is associated with a region of low dynamic perturbation pressure. Interested readers are referred to Klemp (1987) for a complete explanation behind Equation (4). The development of vortices in convectively-driven flow impacts the pressure field. Flow will be accelerated or decelerated by the pressure gradient forces that result. Therefore the one flow feature in fire convection responsible for a **dynamical force** in a fluid is a vortex.

4. EXPERIMENTAL RESULTS

The fire-front positions and total heat-release rates as functions of time for each simulation are shown Figure 3. Figure 3 depicts the average forward movement (solid line) and the total heat-release rates (dashed line) of the CONTROL (purple), SHEAR (navy), LOG (red), and TANH (green) fires. In each fire, the fire-domain total heat-release rates peak with ignition, quickly equilibrate, steadily decline during the first 800 to 1000 seconds, and then level off after that. The larger the fire-spread rate the more intense the fire. Before ~ 1000 seconds, depending on the vertical structure of the background wind, the fire front moves either extremely slowly (e.g., the TANH fire), or slowly (e.g., the SHEAR fire) or very quickly (e.g., the LOG fire), or somewhere in between (e.g., the CONTROL fire), even though the upstream mean near-surface wind of

all fires is the same. From here on “surface” or “near-surface” refer to the 4 m above-ground-level or AGL (the height of second vertical grid level in the WRF-fire model). After 600 s, the strengths of the fire-induced winds and plume updrafts in the CONTROL, SHEAR, and LOG fires decrease gradually with time, as each fire’s head, perimeter, and active burning area narrow and stretch, causing the total fire domain heat-release rate to decline.

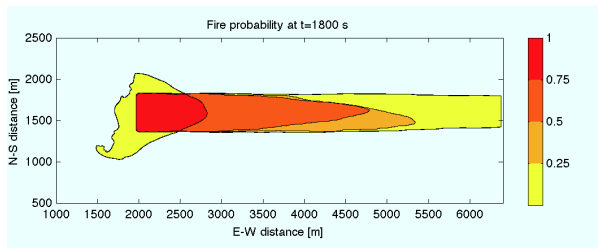


Figure 4: Burn probabilities based on the four experimental fires at the end of the simulations. Initial fireline length was 400 m.

From the very beginning, the TANH fire propagated more slowly than the other fires and evolved in a completely different way. The heat-release rates in the TANH fire decrease with time to almost nil at 900 seconds, and then increase again to match the heat-release rates of the other fires. This heat-release rate behavior is consistent with the relatively slow forward (eastward) propagation of the TANH fire front during the first 900 seconds. Figure 3 indicates, however, that 900 seconds into the simulation is a critical moment in the TANH fire; the forward movement of the fire front stalls and fire-induced surface winds become suddenly extremely erratic. After this point, the TANH fire develops an active fire front in a different section of the fire’s perimeter that moves westward, not eastward.

For the first 1000 seconds, the LOG fire had the fastest forward propagation speed and consequently the greatest heat-release rate. An examination of the rate-of-spread data at 5-second intervals shows that the rate-of-spread at the head of the LOG fire almost always reached the limiting value (approximately 6 m s^{-1}) allowed by the rate-of-spread formulation used in WRF-SFIRE (Mandel et al., 2008, 2011). After 1000 seconds, the LOG fire front was out of the fire domain, which explains why Figure 3 shows a constant fire front position from then on. The LOG fire’s declining total fire-domain heat-release rates in Figure 3 after 1000 seconds are from only the portion of the LOG fire perimeter still within the fire domain.

To illustrate the differences in fire spread and area burned between the four experimental fires, burn prob-

abilities were calculated. Figure 4 shows the final probability distribution of fire spread and area burnt at the end of the fire simulations. A 1.0 means all fires burned that area, 0.75 means three out of four fires burned that area, 0.5 means two out of four fires burned that area, and a 0.25 means one out of four fires burned that area. The outlines are the perimeters of the CONTROL (forward/eastward movement), SHEAR (slowest forward/eastward movement), LOG (fastest forward/eastward movement), and TANH (forward/eastward and then backward/westward movement) fires. The red areas in this figure mean that, no matter what the background wind profile for the fires, this area will burn (100% burn probability). The other colors mean smaller probabilities. The TANH output is shifted to have the ignition line at the same location as the other simulations.

Figure 4 indicates that, from an operational fire-fighting perspective, the SHEAR fire, burning in an ambient wind with slightly negative linear vertical ambient wind shear, was the slowest forward-spreading and “best behaved” fire compared to the others in the study. Figure 4 indicates also that, from an operational fire-fighting perspective, the LOG fire’s propagation was impressively large and steadily forward (eastward), while the TANH fireline’s propagation was highly erratic.

The results of this small sample (only four fires) are, of course, skewed by the rapid propagation of the LOG fire front through the fire model domain and by the backward movement of the TANH fire perimeter. Nonetheless, the probability distribution still serves as an illustration of the kind of variability in fire spread and area burnt that outliers can cause. Figure 4 demonstrates that the fire-induced wind perturbations due to fire-plume/atmosphere interactions are responsible for the variability in rate-of-fire-spread and area burnt. Since the only environmental feature that differed between the four fires was the vertical structure of the above-surface ambient wind shear, this atmospheric condition was therefore inevitably responsible for the uncertainty in fire spread seen in Figure 4.

In order to understand the evident differences between fires seen in Figures 3 and 4, an examination of the surface flow features based on Equations 1, 2, 3, and 4 are presented next. Compared to the CONTROL, the slightly negative vertical shear in the background wind did not impact the SHEAR fire’s behavior in any significant way except that the magnitudes of flow properties and forward fireline propagation are slightly smaller in the SHEAR fire. From here on relevant results from the LOG and TANH fires are described and shown, and the analyses of the CONTROL fire are described but not shown.

4.1 At 5 Minutes – Initial Steady-state

The CONTROL fire (not shown) front has moved about 0.5 km in the positive x direction since ignition. There is strong convergence along the forward fire perimeter and fire head as the fire-induced flow comes together at the base of the fire's convection column. A w maximum at 100 m AGL is 18 m s^{-1} and co-located with the maximum convergence in the near-surface flow below. The w minimum is -4 m s^{-1} and found along the fire's flank. The westerly mean flow is normal to the ignition line, and the fields in the CONTROL fire are symmetrical with respect to the central east-west axis of the fire. The areal extent of the surface flow influenced by the CONTROL fire's convection is approximately half a kilometer ahead, behind, and on either side of the front front.

Three-dimensional animation and examination of the data show that at this time, for every fire, there is a vortex couplet associated with the active fire front. This feature is seen in Figures 5a and 6a. The vortex couplet is two distinct, coherent, nearly equal-magnitude, persistent counter-rotating vertical vortices located at the fire's head that are either embedded in (CONTROL, SHEAR, TANH) or just ahead (LOG) of the fire front (e.g., Figure 5a). The CONTROL fire (not displayed) shows that the cyclonic and anticyclonic rotations of the southern and northern vortices, respectively, of the couplet are almost equal in magnitude and strength (i.e., $\sim 1 \text{ s}^{-1}$ which is tornado-strength). The vortex couplet shapes the fire front, enhances the local surface wind speed, and is often, but not always, strongly co-located with the convergence maxima in the flow (e.g., see Figures 5 and 6). In the CONTROL fire (not shown) the x locations of the two vortices match the x position of the maximum fire-induced surface wind speed (which is almost 18 m s^{-1}) that occurs a little behind the convergence maximum. All four fires show the surface convergence pattern in the near-surface flow in the vicinity of the fire front pulling the fire front into an (almost) parabolic shape. At 300 seconds, for every fire, there is moderately strong divergence in the surface flow approaching the base of the convective updraft, followed by strong convergence in the surface flow just at the tip and ahead of the burning fire front. The positioning of these features are relatively consistent with the idealized surface flow depicted in Figure 1.

There are obvious differences between the surface flow features in the LOG fire compared to the CONTROL. There are: the much larger areal extent of surface flow influenced by the LOG fire (Figure 5c); a different placement and configuration of the vortex couplet and divergence-convergence pattern associated

with the fire front (Figure 5a,b); a deeper fire front; and a greater forward movement of the fire front (approximately 0.85 km in the positive x direction over the last 5 minutes). The LOG fire shows strong surface divergence in the center of the domain accompanied on each side by two symmetrical convergence zones that extend almost 0.5 km ahead of the fire front. Figure 5c shows how much further forward the w at 100 m AGL extends. The areal extent of the surface flow influenced by the LOG fire is nearly a kilometer ahead and behind the front front (Figure 5c).

It is likely that the differences in the surface divergence pattern in the LOG fire compared to any of the other fires are due to the position and strength of the LOG vortex couplet. Compared to the CONTROL fire, the x position of the LOG vortex couplet is out ahead of, not embedded in, the fire front. The x position of the LOG vortex couplet (2.95 km; Figure 5a) matches closely the maximum $|\vec{V}'_H|$ (17.4 m s^{-1} at $x = 2.97$ km; Figure 5c). Unlike the CONTROL fire, the vortex couplet and $|\vec{V}'_H|$ maximum in the LOG fire lead the convergence maxima ($x = 2.87$ km; Figure 5b) by about 100 m. The stronger fire-induced surface winds associated with the vortex couplet are consistent with greater convergence in the surface flow just ahead of the fire front and greater divergence in the surface flow out ahead of that, and are part of the near-surface wind pattern associated with the more near-parabolic shape of the LOG fire front. The distance separating the rotating columns of the vortex couplet is also larger in the LOG fire compared to the CONTROL. Furthermore, the maximum w at 100 m AGL was 19 m s^{-1} at $(x,y) = (3.05, 1.53)$ km, co-located, not with the convergence maximum in the surface flow, but with the x position of the vortex couplet.

Figure 6 shows that, even though the general patterns of vorticity, divergence and wind speed perturbations in the TANH fire resemble the ones from CONTROL fire, there are also obvious differences between them. Magnitudes of flow properties, the areal extent of the surface flow influenced by the fire's convection column, depth of the fire front, and forward fireline propagation are noticeably smaller in the TANH fire compared to the CONTROL. While the CONTROL and LOG fires have propagated by as much as 0.55 and 0.85 km forward, respectively, the TANH fire front has moved only approximately 0.45 km forward. Furthermore, Figure 6c indicates perturbed flow behind (i.e., to the west of) the TANH fire, while in the CONTROL (not shown), SHEAR (not shown), and LOG fires, flows were perturbed only ahead of the fires. In the TANH fire, the strongest w at 100 m AGL, and surface convergence, vorticity, and $|\vec{V}'_H|$ are all located over and along the leading edge of the fire front. In Figure 6c,

the maximum w at 100 AGL was 16 m s^{-1} at $(x,y) = (4.49, 1.57) \text{ km}$, located above the maximum convergence in the surface flow.

The background wind field in the CONTROL fire has no shear, the SHEAR fire has slightly negative linear vertical shear, the LOG fire has large surface positive vertical shear, and the TANH fire has intense negative vertical shear. It can be noted, however, that the directions of rotation in the vortex couplets associated with the fire fronts are the same for all four fires. This suggests that the vertical shear in the background wind is not responsible for the direction of rotation in the vortex couplet and that vorticity of significant magnitude seen in Figures 5a and 6a, and 7a is fire-induced.

Figure 7 shows low pressure perturbations at the base of each vortex in the LOG vortex couplet, consistent with Equation (4). This occurs in every fire. The vortex couplet at the head of each fire impacts the pressure field, providing a eastward-directed pressure gradient force that causes forward motion as the air flows from high to low pressure.

In a uniform flow, two vortices having opposite rotation of equal strength do not rotate around each other, but move along with this flow in straight lines parallel to each other (Markowski and Richardson, 2010). The vortex couplet is expected, therefore, to behave in this fashion unless the wind field that the vortex couplet is embedded in becomes non-uniform (i.e., is perturbed) and/or the rotation rates of the vortices become unequal. Flow-property symmetry with respect to the central east-west axis of the fire is evident in the CONTROL, SHEAR, and LOG fire plumes, less so in the TANH. An analyses of the model output indicates that this asymmetry in the TANH plume at 300 s grows greater over time. It will be shown that this asymmetry to the TANH flow becomes important to the propagation of the vertical vortices and low pressure perturbations (like those seen in Figure 7) associated with the actively moving section of the fire perimeter.

4.2 At 10 Minutes – Steady-State

The properties displayed in Figures 8 and 9 are the same as those displayed in Figures 5 and 6, except for 600 seconds (10 minutes) into the simulations.

A comparison of flow properties for the CONTROL fire at 600 s to those at 300 s shows that the fire front is maintaining its near-parabolic shape, having moved forward by approximately .90 km in the last 5 minutes, with a slight drop in the magnitudes of divergence and wind speed perturbation maxima and minima, while the areal extent of the surface flow influenced by the fire's convection column has grown. The

associated surface convergence in the flow is weaker, the weak convergence in the surface flow out ahead of the CONTROL fire front at 300 s (not shown) is gone, and the maximum in the fire-induced surface wind perturbation has decreased (15.2 m s^{-1} at 600 s versus approximately 17.7 m s^{-1} at 300 s). The flow fields are still symmetrical with respect to the central east-west axis of the fire. The surface strength of the CONTROL vortex couplet is less than it was at 300 s. Even though the general shape of the fire front is conserved, its head is smaller due to a decrease in the size of, and separation distance between, the rotating columns in the vortex couplet.

In the CONTROL fire, as well as the SHEAR and LOG fires, the vertical vortices in the couplet have moved closer to each other; this change is attributed to non-uniformity in the fire-induced flow and the discrepancy in magnitude of rotation between the counter-rotating vortices in the vortex pair. To a great extent, however, the vortex couplet is behaving as expected; the vortices have continued to move parallel to each other, in the same direction as the background (westerly) flow. The reduction in size of the vortices, however, is evident only close to the surface. An examination of the data shows that the columns in the vortex couplet form a narrow V-shape in the vertical, spreading apart further with height; the V-shape configuration gives them more space at higher levels, allowing for their horizontal growth with height.

Near-surface shear in the wind profile in the LOG fire does impact fire behavior and fireline propagation in significant ways. Figure 8 shows that the fire front has moved forward by 1.5 km in the last 5 minutes, and almost all surface flow ahead of the fire combustion is greatly perturbed by strong eddy development in the downstream flow (Figure 8b). Contrary to the CONTROL fire, which shows a decrease in the magnitude of the surface fire-induced wind speed with time, the magnitudes of the LOG surface fire-induced wind speed are increasing with time, reaching a maximum of $\sim 19 \text{ m s}^{-1}$ (Figure 8c) at 600 s. Just as at 300 s, a concentrated, strong, narrow updraft begins close to the surface (Figure 8c). The black lines in Figure 8c are the 9 m s^{-1} contours for w at 100 m AGL. Even though vertical motion is significant, it is found out ahead of the fire front; the maximum w at 100 m AGL was 23 m s^{-1} at $(x,y) = (4.49, 1.61) \text{ km}$, located above the maximum convergence in the surface flow.

Although the strength of the LOG vortex couplet (Figure 8a) is slightly weaker than 5 minutes ago, it is still greater than that of the CONTROL fire. The areal extent of surface flow influenced by the fire's convection column continues to grow (Figure 8c). The fire front shows an almost parabolic shape.

While the strength of the fire-induced updrafts at 5 and 10 minutes in the CONTROL fire was practically the same during the same time interval, the maximum updraft speed in the LOG fire increased from 29 to 34 m s⁻¹. At 600 s into the LOG simulation, the maximum updraft speed is located at 650 m AGL (not shown), while in the CONTROL fire it is located at 1550 m (not shown), almost one kilometer higher. Even though the maximum upward velocity in the LOG fire at 600 s practically matches that in the CONTROL fire (34 versus 33 m s⁻¹), the positioning of the maximum updraft closer to the ground appears to contribute to the LOG fire's more active surface flow features. Near-surface horizontal convergence, important to fireline propagation, is strengthened by the low-level w maximum. The results suggest also that a fire burning in an ambient wind with a near-surface logarithmic wind profile is capable of maintaining stronger surface fire-induced winds and vortex couplet, and therefore a greater spread rate compared to a fire burning in an ambient wind with a constant wind profile.

Figure 9 shows that there is something highly unusual about the TANH fire that cannot be seen or understood by an examination of surface flow properties only. While the CONTROL (not shown) and LOG fires have propagated by as much as 0.9 km and 1.05 km forward, respectively, in the last five minutes, the TANH fire front has moved forward by only 0.6 km. Like the LOG fire, the surface flow ahead of the fire combustion is perturbed by eddy development in the downstream flow (Figure 9b), but with disorganized patterns of weak divergence and convergence, accompanied by weak wind speed perturbations (Figure 9c). Other differences are: the diminished vortex couplet at the head of the fire, and diminished fire-perimeter and flow-property symmetry with respect to the central east-west axis of the fire (Figure 9a); the development of concentrated but relatively weak positive/negative vertical vorticity (Figures 9a,b); and a weakly perturbed surface wind almost everywhere in the model domain (Figure 9c). The shape of the TANH fire front is no longer parabolic-like.

Two counter-rotating columns have formed roughly 300 m ahead of the TANH fire front (Figure 9a), and their rotations are both stronger than, and opposite in sign to, the rotations in the vortex couplet at the fire's head. These vortices are accompanied by $|\vec{V}'_H|$ values of approximately 10 m s⁻¹ (Figure 9c). Examination of the data shows that an additional ten-or-so more weakly rotating vertical vortices formed even further downwind, and the bases of these are seen on the right in Figure 9a.

An inspection of the data indicates that the strongest TANH updraft occurs at ≈ 460 m AGL (not

shown), lower than in the LOG or CONTROL fire plumes. The solid black lines in Figure 9c show the 5 m s⁻¹ contour for w , the vertical wind component at 100 m AGL. The maximum w at 100 m AGL was 12 m s⁻¹ at $(x,y) = (4.75, 1.55)$ km, and the minimum w was -4 m s⁻¹ at $(x,y) = (4.63, 2.01)$ km. The TANH fire plume tilts significantly backward (upstream against the surface wind; not shown), and its maximum upward velocity is severely reduced compared to what it was 5 minutes ago (i.e., 18 m s⁻¹ vs. 32.3 m s⁻¹), and accompanied by a substantial drop in the magnitude of the surface wind speed perturbations (Figure 9c).

The disturbed flow ahead of the fire front may be partly fire-induced or partly be due to the shear-flow instability that can develop between the eastward moving surface wind layer and the westward moving upper-level wind (Figure 2; TANH ambient wind profile). The complex pattern of surface divergence (Figure 9b) is not present in the surface flow of the other fires. Analysis of the TANH data suggests that this pattern is associated with the existence of horizontal rolls within the first 200 m above the surface which may have been triggered by the (almost) symmetrical eddies that formed on both sides of the plume (not shown). However Figure 9c indicates irregular surface flow throughout the fire domain, and it is not unreasonable to attribute these departures from the ambient wind to inherent instability in the background tanh wind profile (Brown, 1972).

4.3 At 15 Minutes – End of Eastward Propagation of TANH Fire

The properties displayed in Figures 10 and 11 are the same as those displayed in Sections 4.1 and 4.2 except for 900 seconds (15 minutes) into the simulations.

The CONTROL fire (not displayed) at 900 s shows that the near-parabolic shape of the fire front is narrowing. The fire front has moved forward by approximately .80 km in the last 5 minutes. There are further slight decreases in the magnitudes of the surface flow properties. Flow properties are still symmetrical with respect to the central east-west axis of the fire. The surface strength of the vortex couplet continues to decrease while the areal extent of the surface flow influenced by the fire's convection column has grown moderately over the last 5 minutes.

Figure 10 shows that the LOG fire front has almost reached the east boundary of the fire domain and its propagation has slowed down somewhat; it has moved forward by 1.4 km in the last 5 minutes compared to 1.5 km in the previous 5-minute interval. The areal extent of surface flow influenced by the fire's convection

column continues to grow (Figure 10c). A larger area upstream of the fire front is perturbed (Figure 10b), but the maximum wind speed perturbation is smaller than before: 6.37 m s^{-1} in Figure 10c versus 18.8 m s^{-1} in Figure 8c. The solid black lines in Figure 10c show the 7 m s^{-1} contour for w , the vertical wind component at 100 m AGL. The maximum w at 100 m AGL was 12 m s^{-1} at $(x,y) = (6.13, 1.77) \text{ km}$, and the minimum w was -2 m s^{-1} at $(x,y) = (6.13, 1.69) \text{ km}$. And while the strength of the vortex couplet is slightly weaker than it was 5 minutes ago, it is still greater than that of the CONTROL fire. Just as for the CONTROL fire, an examination of the above-surface data shows the columns in the vortex couplet forming a V-shape in the vertical, spreading apart further with height. According to these surface properties, the LOG fire can be described as a near-steady-state but actively-moving fire; it took 15 minutes for this fire's front to travel approximately 4.5 km forward to reach the eastern edge of the fire model domain.

The TANH fire continues to behave erratically (Figure 11); any organization or symmetry in the flow patterns associated with the fire perimeter has disappeared. The fire front has effectively stopped propagating in the positive x direction, in agreement with Figure 3 where forward movement of the TANH fire is seen to stall at 900 seconds. The perturbed surface horizontal wind field has strengthened, reaching maximum speeds of 14 m s^{-1} (Figure 11c), and includes multiple regions of divergence/convergence downwind of the fire (Figure 11b). Remarkably $|\vec{V}_H'|$ values are over 10 m s^{-1} on the western side ($x \leq 2.5 \text{ km}$) of the fire model domain. The solid black lines in Figure 11c show the maximum w at 100 m AGL is only 8 m s^{-1} and located at $(x,y) = (5.59, 1.89) \text{ km}$, in the upper right of the plot, a considerable distance away from the burning fire perimeter. A minimum w of -7 m s^{-1} is located at $(x,y) = (5.43, 1.87) \text{ km}$, nearby the maximum w in Figure 11c.

Figure 11a,b and Figure 12 is showing dynamical activity along the TANH rear perimeter; i.e., significant vertical vorticity accompanied by negative pressure perturbations and convergence are impacting the shape and depth of the fire perimeter there. This rear-fire development is not shared by the other fires.

4.4 At 20 Minutes – Westward Propagation of TANH Fire

The properties displayed in Figure 13 are the same as those displayed in Sections 4.1 to 4.3 except for 1200 seconds (20 minutes) into TANH simulation.

The CONTROL fire (not displayed) at 1200 s shows a now narrow “pinched” fire front that has moved for-

ward by approximately .54 km in the last 5 minutes. There are further slight decreases in the magnitudes of the surface flow properties. Flow properties are still strongly symmetrical with respect to the central east-west axis of the fire. The vortex couplet at the fire front is not apparent in the surface flow. Examination of above-surface flow shows that the columns in the vortex couplet still exist and form a V-shape in the vertical, but no longer extend to the surface; and this vortex configuration continues until the end of the CONTROL simulation.

The fast-moving fire front of the LOG (not shown) fire has exited the fire model domain; the areal extent of surface flow perturbed by the fire remains large. The most notable difference from an operational fire-fighting perspective between the behavior of the LOG fire and the CONTROL is the rapid propagation speed of the LOG fire front eastward.

The surface properties of TANH displayed in Figure 13 show even greater irregularity. Examination of the data shows that vertically-rotating columns (vortices) have formed almost everywhere throughout the model domain. The fire front is not propagating in the positive x direction. Animations of plots of these surface properties show several concentrated regions of negative ζ^z , with attendant regions of convergence, developing and moving in and around the western region of the TANH fire perimeter. The contours (red lines) delineating the fire perimeter in Figure 13 show this section of the fire perimeter expanding westward and southwestward. The wind vectors inside the fire perimeter show that the surface flow has reversed direction completely; they point west instead of east. An observer on the ground would risk being buffeted by the rapidly changing winds around the TANH fire.

4.5 At 25 Minutes – South-Westward Propagation of TANH Fire

The results displayed in Figure 14 are similar to those displayed in Sections 4.1 to 4.4 except that they are for 1500 seconds (25 minutes) into the TANH simulation. Analysis of the LOG fire (not displayed) shows that at this time and to the end of the simulation, forward movement of the fire front continues. The CONTROL fire (not displayed) shows an even more “pinched” fire-front shape that has moved forward by 0.54 km in the last 5 minutes, and there are further slight decreases in the magnitudes of the surface flow properties. Flow properties continue to show symmetry with respect to the central east-west axis of the fire.

The surface properties of TANH displayed in Figure 14 show that the TANH fire has again changed considerably in the last 5 minutes. The fire front is not

propagating in the positive x direction. The most active section of the fire perimeter in the south-west portion is the new fire front. Animations of plots of the surface properties show several concentrated regions of negative ζ^z (Figure 14a), with attendant regions of convergence (Figure 14b), developing and moving in and spiraling around this section of the fire perimeter. The strongest clockwise-rotating vortex (at $x= 3.91$ km in Figure 14a) is found near the strongest convergence (at $x= 3.93$ km in Figure 14b) just ahead of the strongest wind speed perturbation (at $x= 3.89$ km in Figure 14c) making this the most active section of the TANH fire perimeter. Three-dimensional animations of the model data show that these multiple concentrated regions of extreme ζ^z are vertical vortices. The wind vectors show flow outside the fire's perimeter moving into the fire area, following the spiralling motion in the x - y plane induced by the vertical vortices. Figure 14c shows wind speed perturbations associated with these vertical vortices reaching 13 m s^{-1} . The red contours drawn in Figure 14 to delineate the TANH fire's perimeter show that this section of the fire perimeter has expanded south-westward, while the black contours of w at 100 m AGL in Figure 14c outline the base of the fire plume in the same location.

4.6 End of Simulations – Continued South-Westward Propagation of TANH Fire

The properties displayed in Figure 15 are the same as those displayed in Section 4.5 except for 1795 seconds (30 minutes) into the TANH simulation.

There are no remarkable differences between the CONTROL fire at 1800 s compared to the CONTROL at 1500 s except that there has been a slight loss of symmetry with respect to the central east-west axis of the fire, and this appears as a slight veering to the south-east by the CONTROL fire head.

Once more, three-dimensional animations of plots of the TANH fire show active multiple vertical vortices (Figure 15a), and those developing and moving in and spiraling around the south-western region of the TANH fire perimeter have influenced the flow to produce the change in fire perimeter seen in Figure 15. The wind speed perturbations (Figure 15a) associated with the most active and intense vertical vorticity (Figure 15a) and surface convergence (Figure 15b) reached magnitudes of 16 m s^{-1} . These flow features make the south-western region of the TANH fire perimeter the most active section of the fire. The black contour lines of w at 100 m AGL in Figure 15c show no one single well-defined base of a fire plume. The behavior of this fire and its perimeter is extremely erratic, and an

observer on the ground would not necessarily be safe to have remained along the flanks or even behind the original fireline. The change from the forward-moving TANH fire at 5 minutes (Figure 6) to the fire at 30 minutes (Figure 15) is dramatic.

The reason for the south-westward expansion of the fire perimeter is seen in Figure 16 and explained by Equation (4). The negative pressure perturbation that accompanies the strong vertical vortex at $x,y= 3.91,1.19$ km is responsible for providing the flow forcing that draws the fire perimeter in this direction.

5. CONCLUSIONS

In this study, the WRF-SFIRE coupled fire/atmosphere LES is used to investigate the impact of a single environmental variable, the vertical shear in a unidirectional ambient wind field, on fireline propagation. By selectively varying the ambient vertical wind profile, we examine, through comparative numerical simulations under idealized atmospheric forcing, the influence of four different background vertical wind profiles — all with an identical upstream near-surface wind speed — on the evolution of the spread of the surface fire perimeter.

By examining the surface flow properties we demonstrate that: (1) Fireline propagation in each fire differed considerably; (2) Numerical model prediction of wildfire behavior and propagation cannot be “accurate” unless the coupling between the entire fire, including its plume, and the atmosphere is accounted for; (3) There are certain persistent and consistent flow features fundamental to the plume interaction with the background wind profile that appear to be connected with fire propagation; (4) One flow feature common to the propagating portion of a fireline appears to be vertical vorticity. Persistent and substantial vertical vortices are observed along the active portions of the firelines (i.e., fire head, fire front).

A vortex is a dynamical feature known to provide the pressure differences (gradients) that spread and accelerate fluid flow. A reason suggested for the steady-state fire front propagation in CONTROL, SHEAR, and LOG fires is the fairly unperturbed background flow in each. The vortices in the vortex couplet rotated relatively steadily in opposite directions, maintaining a relatively constant distance between each. They did not move away from or rotate around each other. They moved along with the background flow that remained fairly symmetric along the east-west axis of the fires. The vortex couplet is expected to continue this behavior unless the wind field that the vortex couplet is embedded in becomes non-uniform (i.e., is perturbed) and/or the rotation rates of the vortices become un-

equal. It appears that this scenario was not true in the TANH fire. The vortex couplet that developed in the very early stages was disrupted by the highly perturbed background flow, and the result was erratic fire perimeter propagation. The TANH fire developed highly perturbed background flow because that kind of vertical wind shear is unstable to perturbations in the background flow (Brown, 1972). Although the results of this study support this fluid dynamical explanation for fire perimeter propagation, much more study is required however to completely understand and explain all the physical aspects of this explanation.

ACKNOWLEDGMENTS. This research was supported in part by United States Department of Agriculture Forest Service Research Joint Venture Agreement 03-JV-11231300-08, in part by Department of Commerce, National Institute of Standards and Technology (NIST), Fire Research Grants Program, Grant 60NANB7D6144, and in part by a grant from the Natural Sciences and Engineering Research Council of Canada. A gratis grant of computer time from the Center for High Performance Computing, University of Utah, is gratefully acknowledged.

References

- Bluestein, H., J. LaDue, H. Stein, D. Speheger, and W. Unruh, 1993: Doppler radar wind spectra of supercell tornadoes. *Mon. Wea. Rev.*, **121**, 2200–2221.
- Brown, R., 1972: On the physical mechanism of the inflection point instability. *J. Atmos. Sci.*, **29**, 984–986.
- Cheney, P., J. Gould, and C. W.R., 1993: The influence of fuel, weather and fire shape variables on fire-spread in grasslands. *International J. Wildland Fire*, **3(1)**, 31–44.
- Clark, T., M. Jenkins, J. Coen, and D. Packham, 1996a: A coupled atmosphere-fire model: Convective feedback on fire-line dynamics. *J. Appl. Meteor.*, **35**, 875–901.
- Clark, T., M. Jenkins, J. Coen, and D. Packham, 1996b: A coupled atmosphere-fire model: Role of the convective froude number and dynamic fingering at the fireline. *International J. Wildland Fire*, **6**, 177–190.
- Klemp, J., 1987: Dynamics of tornadic thunderstorms. *Ann. Rev. Fluid Mech.*, **19**, 369–402.
- Klemp, J., and D. Lilly, 1978: Numerical simulation of hydrostatic mountain waves. *J. Atmos. Sci.*, **35**, 78–107.
- Mandel, J., J. Beezley, L. Cobb, and A. Krishnamurthy, 2008: A wildland fire model with data assimilation. *Mathematics and Computers in Simulation*, **79(3)**, 584–606.
- Mandel, J., J. Beezley, and A. Kochanski, 2011: Coupled atmosphere-wildland fire modeling with wrf 3.3 and sfire. *Geoscientific Model Development*, **4**, 1–20 doi:10.5194/gmd-4-1-2011.
- Markowski, P., and Y. Richardson, 2010: *Mesoscale Meteorology in Midlatitudes*. Wiley-Blackwell, 430 pp, first edition.
- Wang, W., Bruyère, M. Duda, J. Dudhia, H. Gill, J. Lin, J. Michalakes, S. Rizvi, and X. Zhang, 2009: ARW Version 3 Modeling System User's Guide. Technical report, National Center for Atmospheric Research, 310 pp.

Log Time[**min:sec**] = 5: 0 at $z = 4$ m

5/ 5 m s⁻¹ ↗

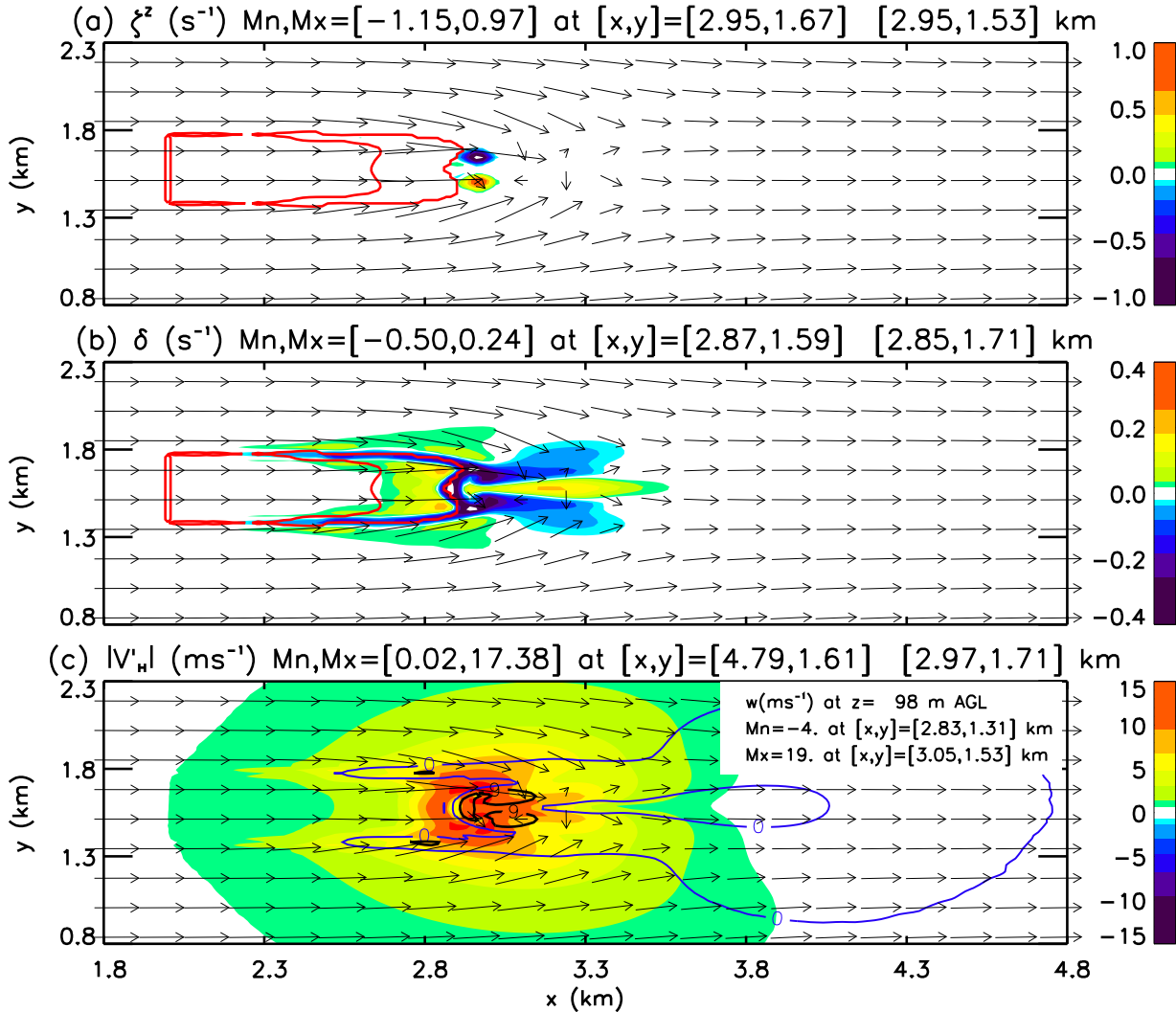


Figure 5: Horizontal x - y cross sections for $z = 4$ m of (a) vertical z vorticity ζ^z (s^{-1}), (b) horizontal divergence δ (s^{-1}), and (c) wind speed perturbations $|V'_H|$ ($m s^{-1}$) at 300 seconds for the LOG fire. Magnitudes of each contour are indicated by colors in bar plots on the right. For each field, minimum and maximum values, plus their (x,y) positions on cross section are given. Vectors denote background plus perturbed wind components in x - y plane where magnitude is scaled as indicated in top right corner of plot. Red contours in (a) and (b) outline the fire (i.e., burning surface area) perimeter. Contour lines in (c) delineate negative (dashed blue), zero (solid blue), and positive (solid black) vertical velocity component w values at approximately 100 m AGL. Note that the (aspect) ratio between the width of the image to its height is not equal to one; consequently all plots show features lengthened in the horizontal direction compared to the vertical direction.

Tanh Time[**min:sec**] = 5: 0 at z= 4 m

5/ 5 m s⁻¹ \uparrow

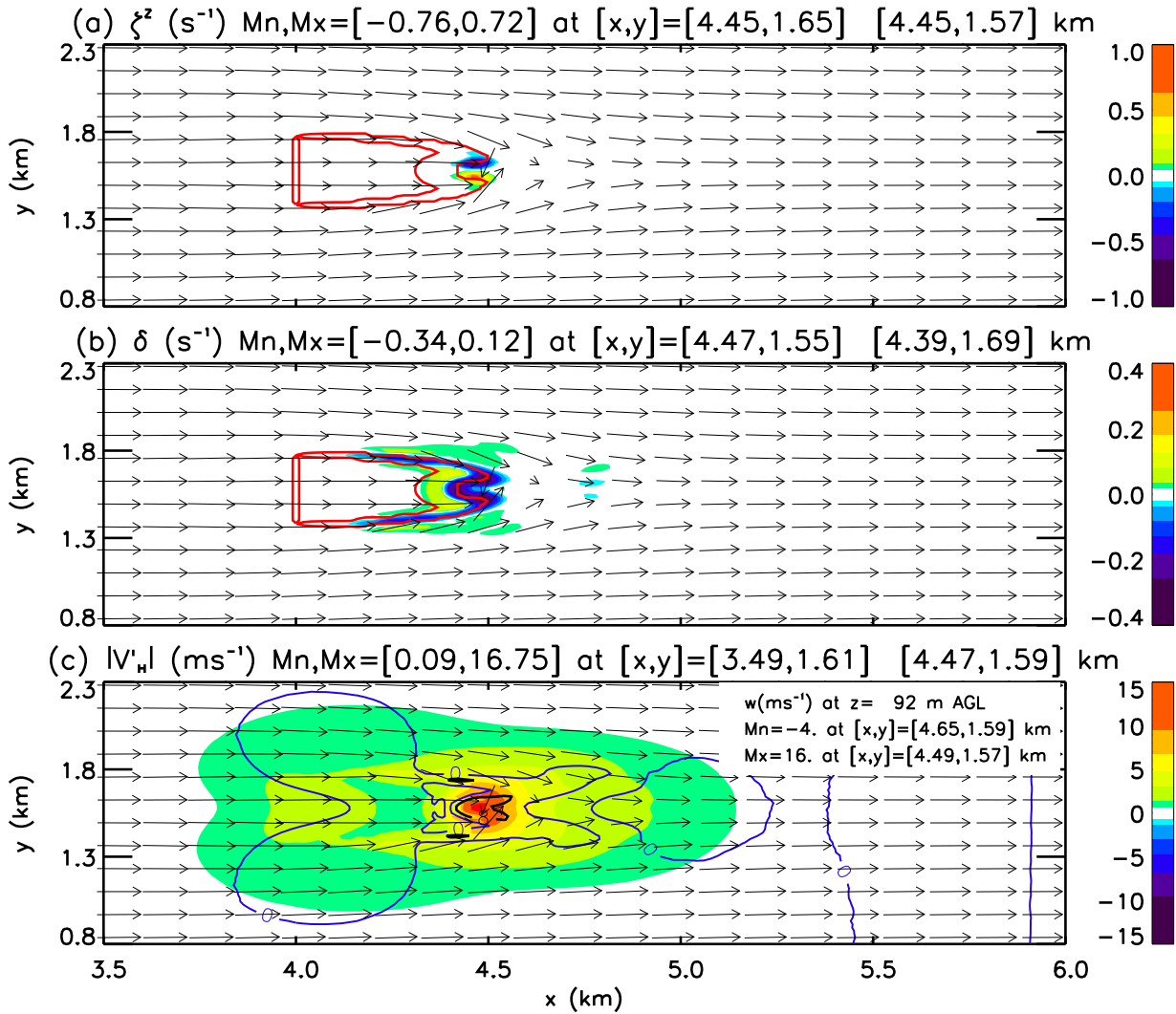


Figure 6: As in Figure 5 except for 300 s into the TANH fire simulation.

Log Time[$\text{min}:\text{sec}$] = 5: 0 at $z(\text{m})= 31$

5/ 5 m s^{-1} \uparrow

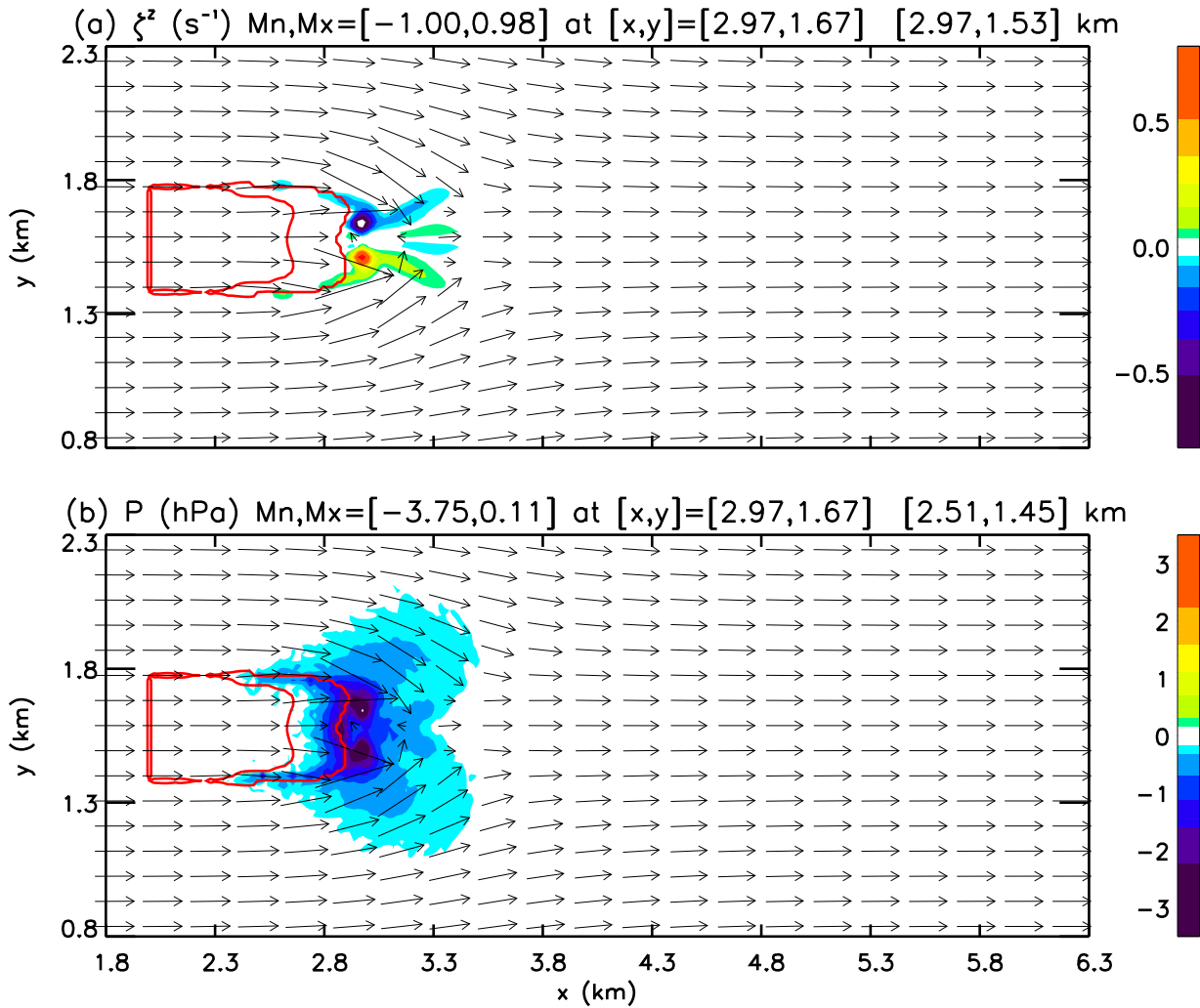


Figure 7: As in Figure 5 except for horizontal x - y cross sections for $z=31$ m of (a) vertical z vorticity ζ^z (s^{-1}) and (b) pressure p perturbations (hPa) at 300 seconds for the LOG fire.

Log Time[**min:sec**] = 10: 0 at z= 4 m

5/ 5 m s⁻¹ ↗

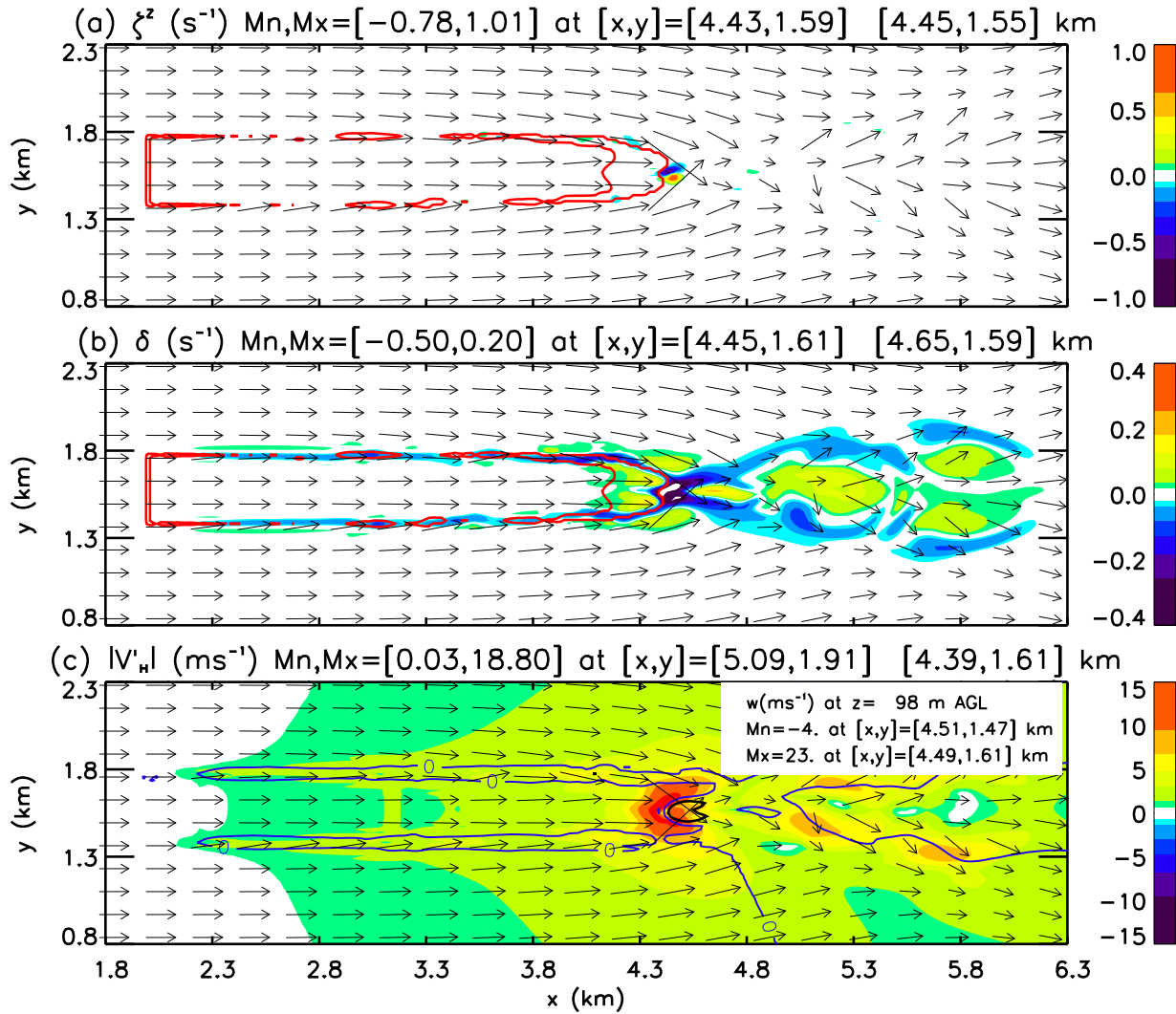


Figure 8: As in Figure 5 except for 600 s into the LOG simulation.

Tanh Time[**min:sec**] = 10: 0 at z= 4 m

5/ 5 m s⁻¹ ↗

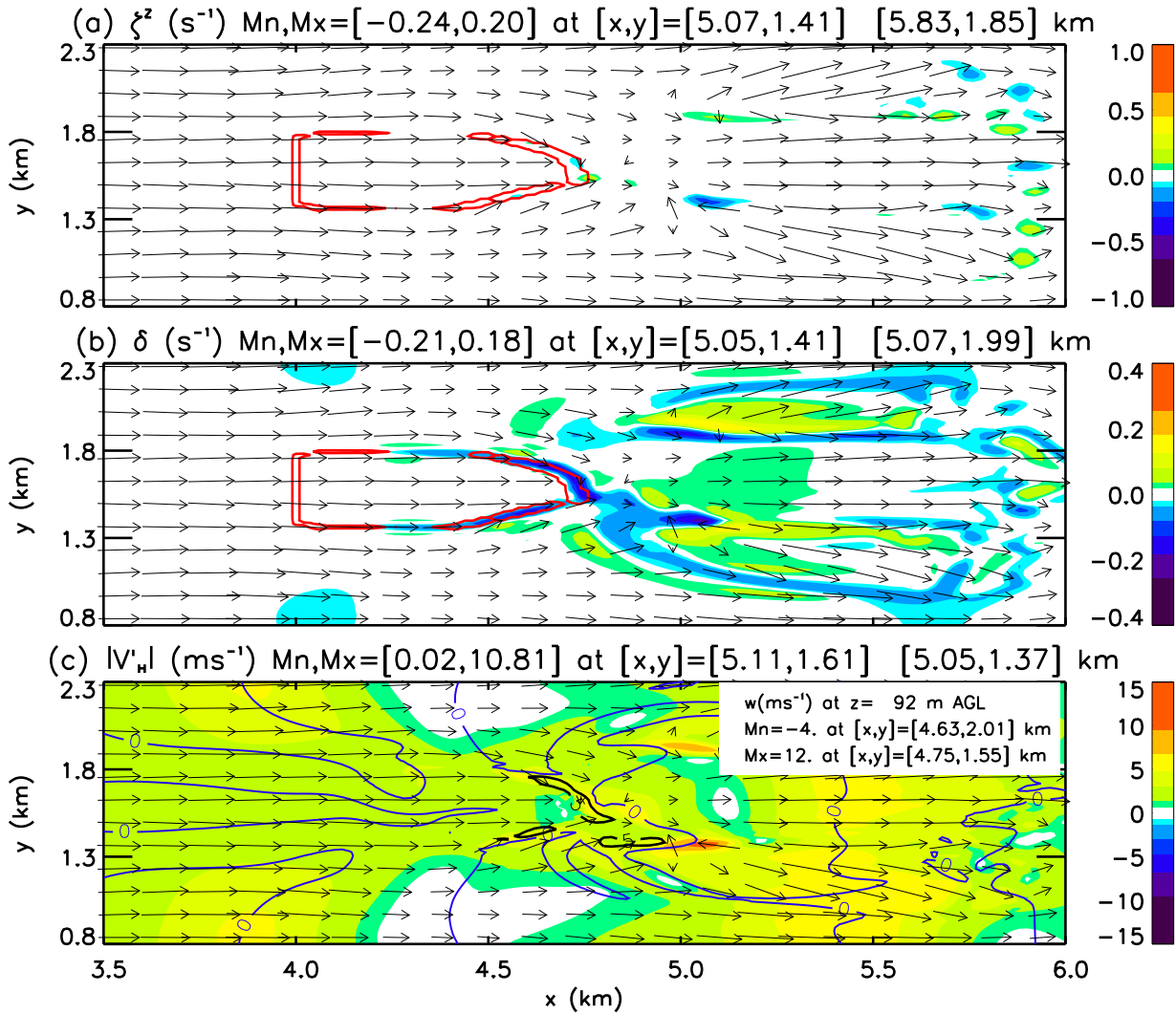


Figure 9: As in Figure 8 except for 600 s into the TANH fire simulation.

Log Time[**min:sec**] = 15: 0 at z= 4 m

5/ 5 m s⁻¹ ↗

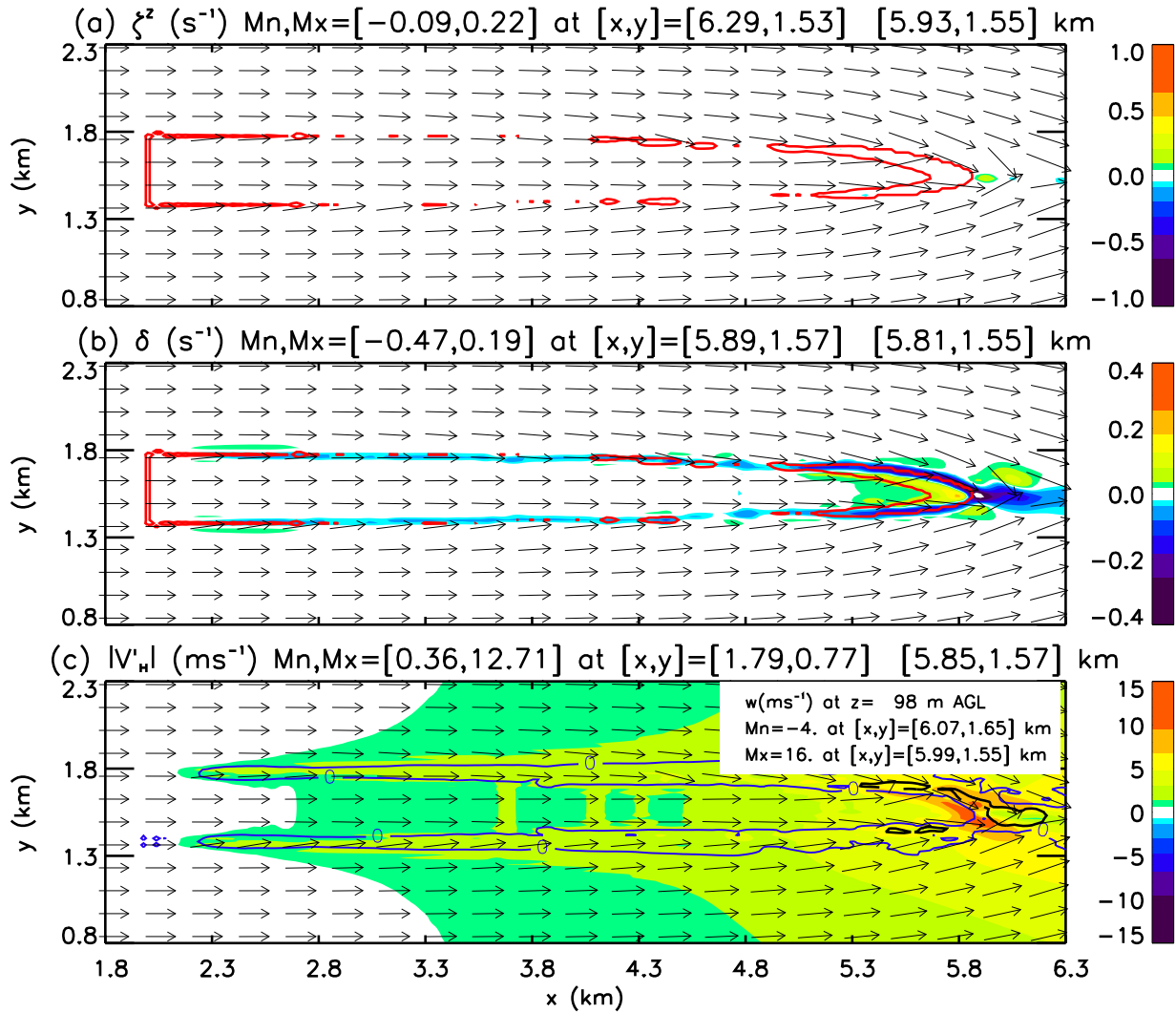


Figure 10: As in Figures 5 and 8 except for 900 s into the LOG simulation.

Tanh Time[**min:sec**] = 15: 0 at z= 4 m

5/ 5 m s⁻¹ ↗ ↘

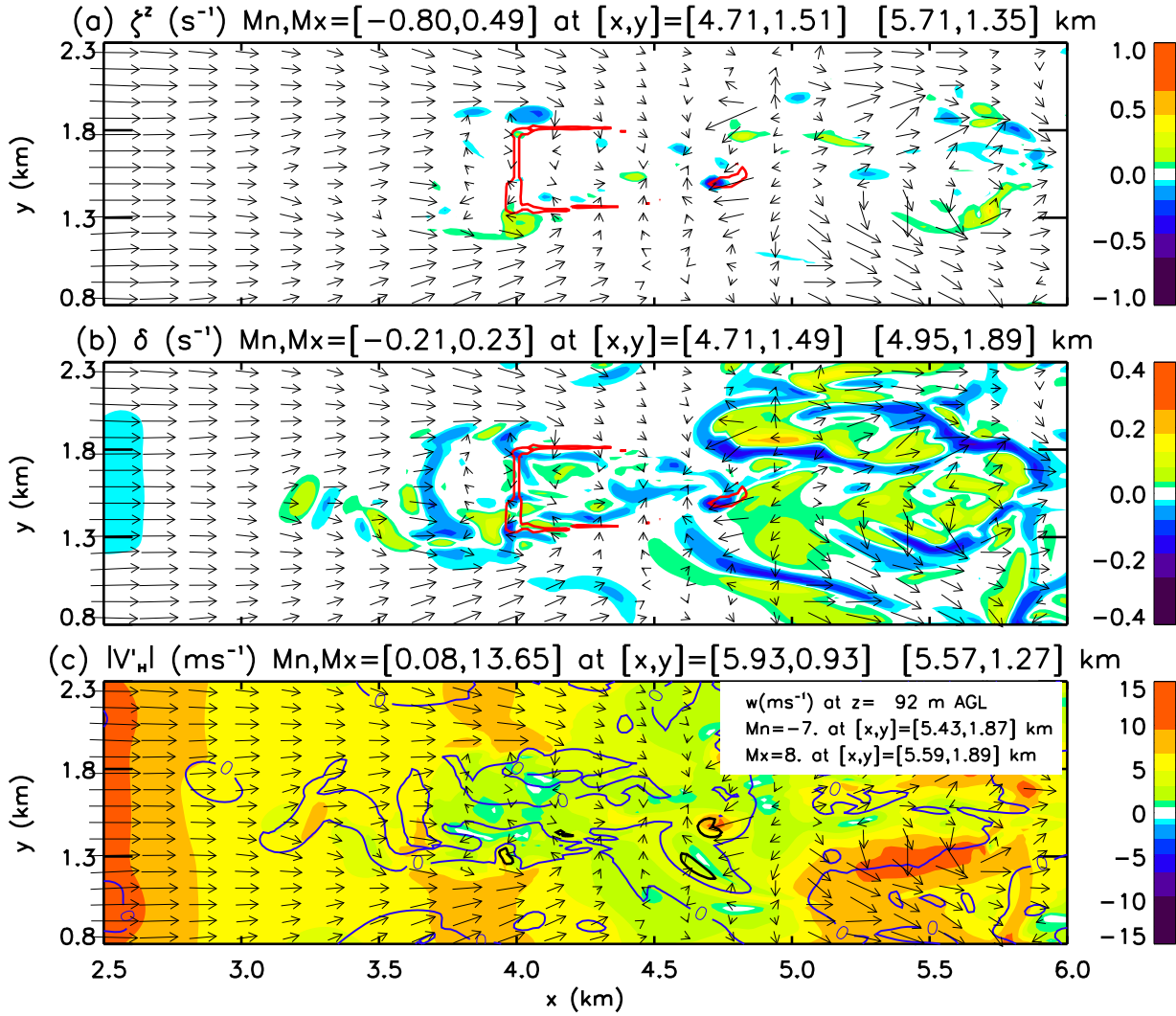


Figure 11: As in Figures 6 and 9 except for 900 s into the TANH fire simulation.

Tanh Time[min:sec] = 15: 0 at z(m)= 32

5/ 5 m s⁻¹ ↗

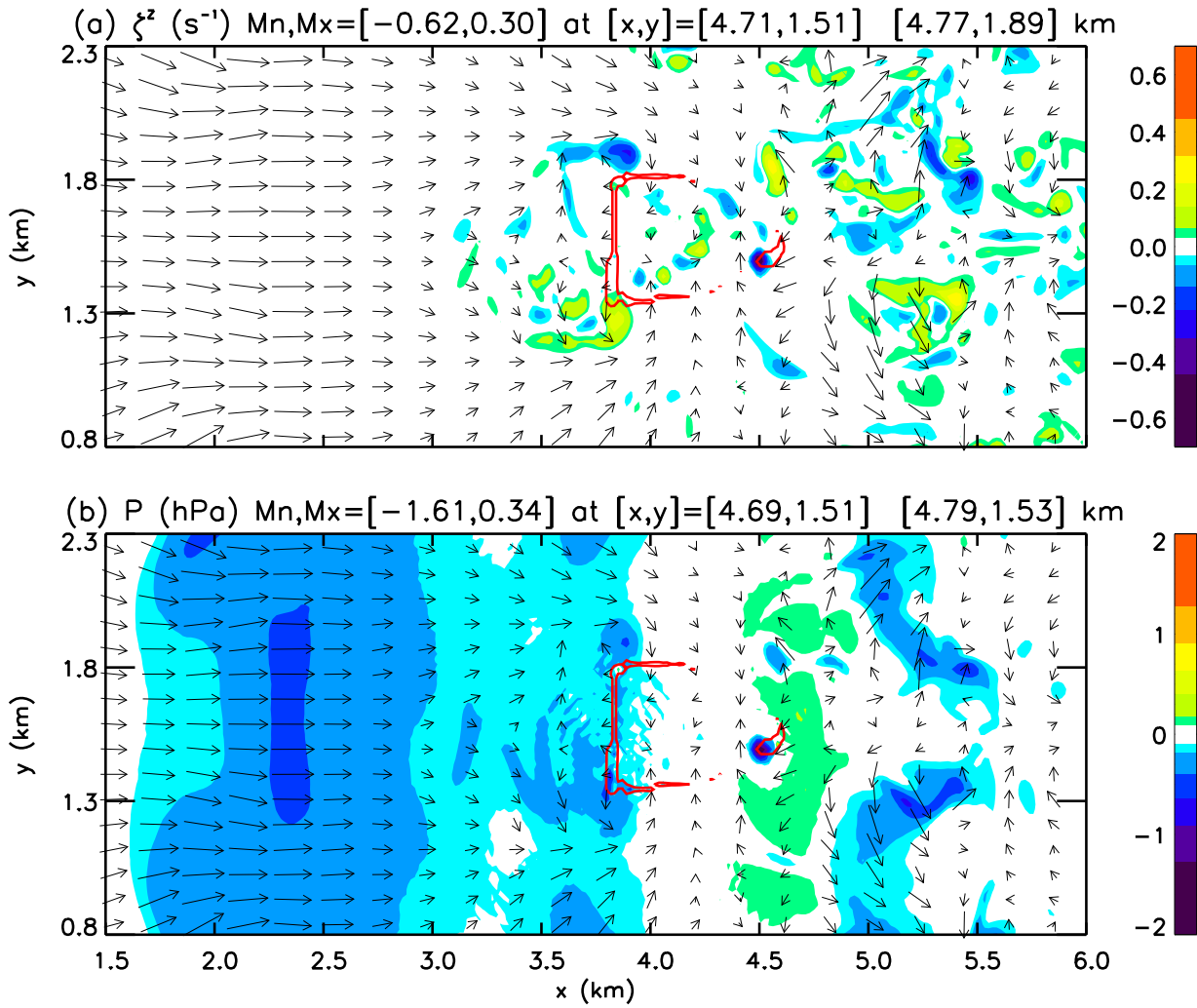


Figure 12: Horizontal x - y cross sections for $z=32$ m of (a) vertical z vorticity ζ^z (s⁻¹) and (b) pressure p perturbations (hPa) at 900 seconds for the TANH fire.

Tanh Time[**min:sec**] = 20: 0 at z= 4 m

5/ 5 m s⁻¹ ↗

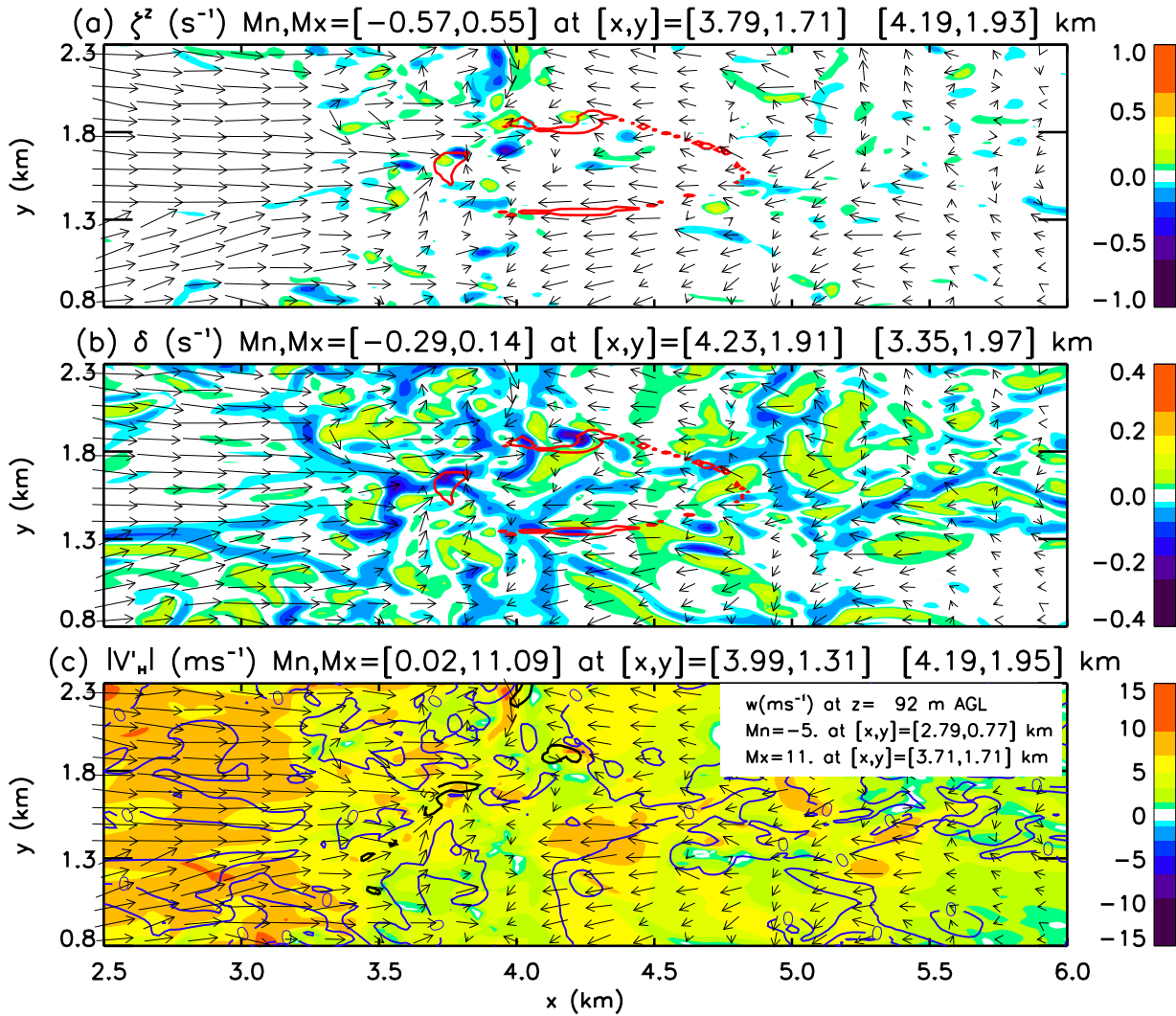


Figure 13: As in Figure 11 except for 1200 s into the TANH fire simulation.

Tanh Time[**min:sec**] = 25: 0 at z= 4 m

5/ 5 m s⁻¹ ↗ ↘

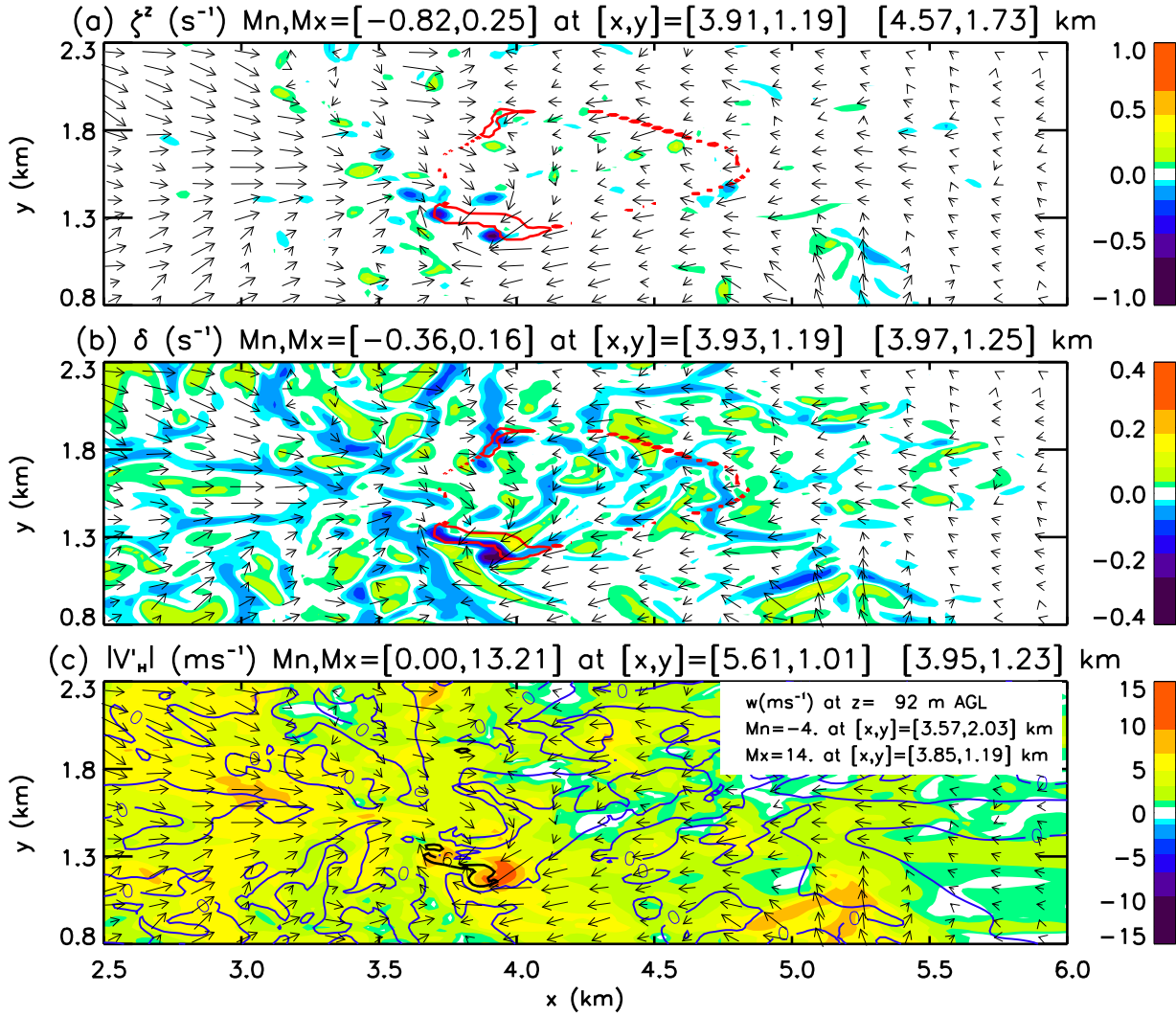


Figure 14: As in Figure 13 except for 1500 s into the TANH fire simulation.

Tanh Time[**min:sec**] = 29:55 at z= 4 m

5/ 5 m s⁻¹ ↗

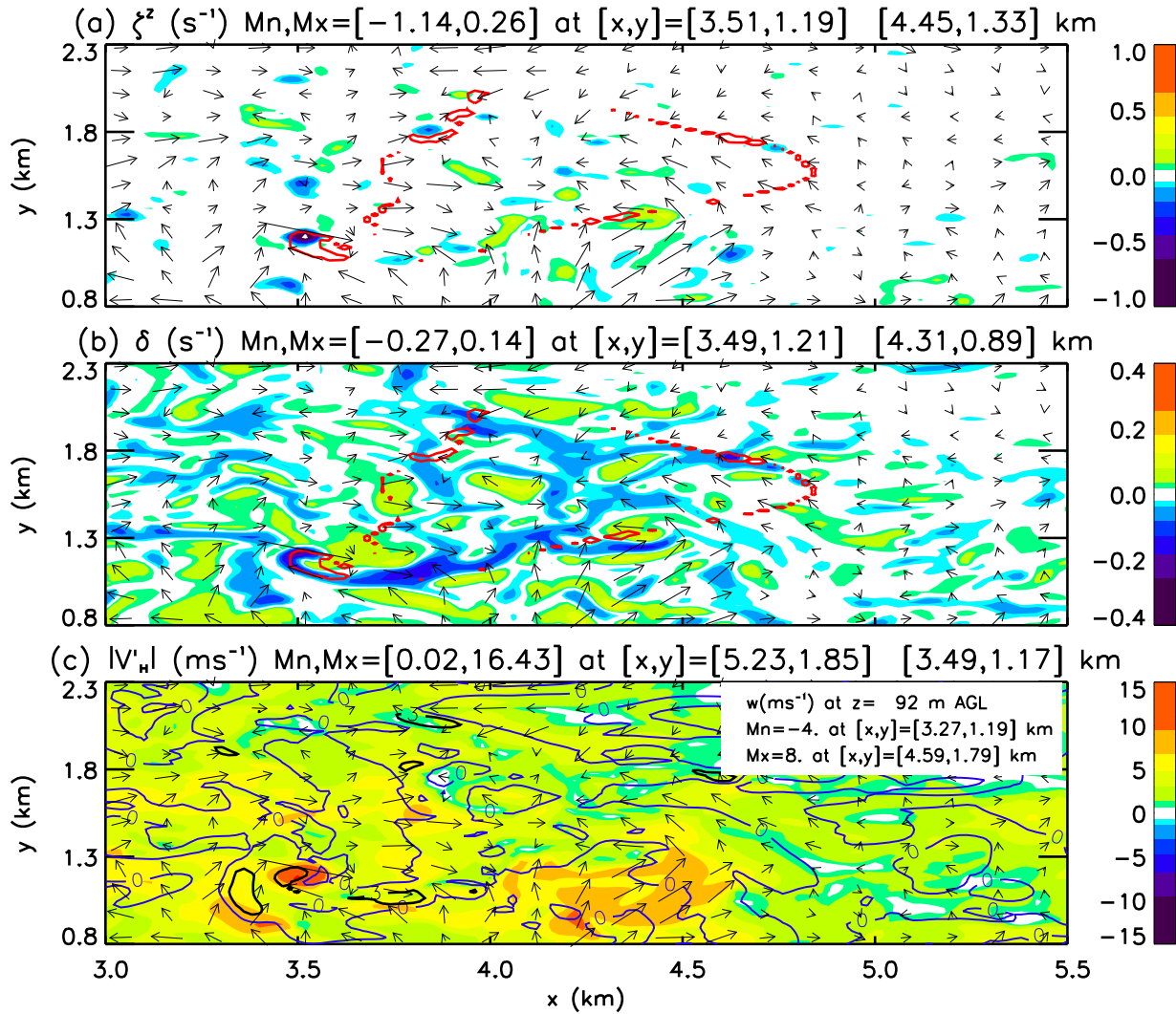


Figure 15: As in Figure 14 except for the TANH fire at the end of the simulation.

Tanh Time[min:sec] = 24:55 at z(m)= 32

5/ 5 m s⁻¹ ↗

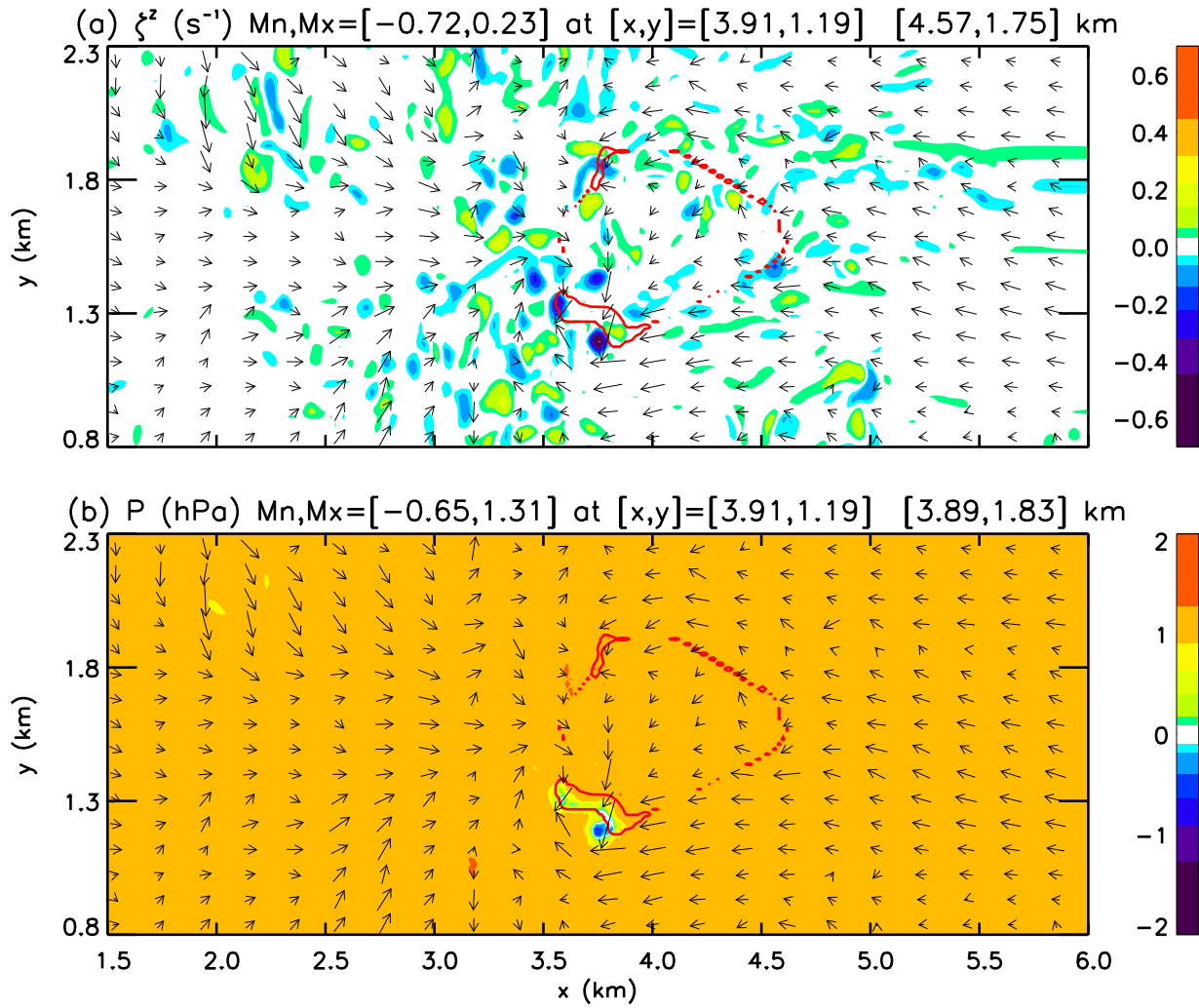


Figure 16: As in Figure 12 except for the TANH fire at the end of the simulation.